Low collectivity of the 2_1^+ state of ^{212}Po

D. Kocheva,[1] G. Rainovski,[1] J. Jolie,[2] N. Pietralla,[3] A. Blazhev,[2] R. Altenkirch,[2] S. Ansari,[2] A. Astier,[4] M. Bast,[2] M. Beckers,[2] Th. Braunroth,[2] M. Cappellazzo,[2] A. Dewald,[2] F. Diel,[2] M. Djongolov,[1] C. Fransen,[2] K. Gladnishki,[1] A. Goldkuhle,[2] A. Hennig,[2] V. Karayonchev,[2] J. M. Keatings,[5] E. Kluge,[2] Th. Kröll,[3] J. Litzinger,[2] K. Moschner,[2] C. Müller-Gatermann,[2] P. Petkov,[6] M. Scheck,[5] Ph. Scholz,[2] T. Schmidt,[2] P. Spagnoletti,[5] C. Stahl,[3] R. Stegmann,[3] A. Stolz,[2] A. Vogt,[2] N. Warr,[2] V. Werner,[3] D. Wölk,[2] J. C. Zamora,[3] K. O. Zell,[2] V. Yu. Ponomarev,[3] and P. Van Isacker[7]

[1]*Faculty of Physics, St. Kliment Ohridski University of Sofia, 1164 Sofia, Bulgaria*

[2]*Institut für Kernphysik, Universität zu Köln, D-50937 Cologne, Germany*

[3]*Institut für Kernphysik, Technische Universität Darmstadt, D-64289 Darmstadt, Germany*

[4]*CSNSM, IN2P3/CNRS and Universite Paris-Sud, F-91405 Orsay Campus, France*

[5]*University of the West of Scotland, PA1 2BE Paisley, United Kingdom and SUPA, Glasgow G12 8QQ, United Kingdom*

[6]*National Institute for Physics and Nuclear Engineering, R-77125 Bucharest-Magurele, Romania*

[7]*Grand Accélérateur National d'Ions Lourds, CEA/DRF-CNRS/IN2P3, Bd. Henri Becquerel BP 55027, F-14076 Caen, France*

(Received 23 June 2017; published 5 October 2017)

The lifetime of the 2_1^+ state of ^{212}Po was measured in the ^{208}Pb(^{12}C,^{8}Be)^{212}Po transfer reaction by γ-ray spectroscopy employing the recoil distance Doppler shift (RDDS) method. The derived absolute $B(E2)$ value of 2.6(3) W.u. indicates a low collectivity and contradicts previous claims of α-cluster components in the structure of the 2_1^+ state. It is demonstrated that a consistent description of the properties of the $2_1^+ - 4_1^+ - 6_1^+ - 8_1^+$ sequence in ^{212}Po cannot be achieved in the framework of a single-j shell-model calculation, either. This puzzle is traced to the properties of the seniority-2 configurations in ^{210}Pb and ^{210}Po.

DOI: 10.1103/PhysRevC.96.044305

I. INTRODUCTION AND MOTIVATION

Single-particle motion and nuclear collectivity are the two extremes which have shaped our understanding of the dynamics for the nuclear many-body system. The nuclear shell model provides the basic framework for understanding of the single-particle motion in nuclei [1]. The collective behavior in open-shell nuclei is understood as a result of coherent movement of valence nucleons caused by the residual interaction, dominated by the proton-neutron interaction [2]. However, the quantitative understanding of the evolution between these two extremes is still not achieved because of the fact that it is sensitive to the structure of the valence space and different components of the effective interaction. In this regard, properties of open-shell nuclei with only two valence proton particles (holes) and two valence neutron particles (holes) with respect to double-magic cores are of particular importance. Such nuclei can often be understood well within the framework of the shell model and at the same time the numbers of the valence particles are large enough to induce the onset of collective behavior. The nucleus ^{212}Po has two valence protons and two valence neutrons with respect to the doubly magic core ^{208}Pb, thus providing a fertile testing ground for studying the beginning of the evolution from single particle to collective motion in the mass $A \approx 208$ region.

Early studies of low-lying structures of ^{212}Po have been aided by the discovery of a high-spin isomer [3]. In an attempt to calculate the spin parity of this isomer in the framework of an extreme shell-model approach, Auerbach and Talmi [4] have also suggested that the yrast sequence $2_1^+ - 4_1^+ - 6_1^+ - 8_1^+$ of ^{212}Po follows a seniority-like energy pattern resulting in an isomeric 8_1^+ state. The isomeric nature of the 8_1^+ state was later confirmed in a series of α- and γ-spectroscopy studies [5]. A complete level scheme of ^{212}Po deduced from a γ-γ coincidence experiment was reported later on by Poletti *et al.* [6] together with the lifetimes of the 6_1^+ and the 8_1^+ states. Up to now, this level scheme has undergone numerous checks [7] and can be considered as well established. However, crucial experimental information on the lifetimes of the 2_1^+ and the 4_1^+ states is still missing [7].

The efforts to understand the yrast sequence of ^{212}Po in the framework of shell models have emphasized [8,9] the importance of configuration mixing but also have revealed a discordance that, while the energies of the yrast states of ^{212}Po are well reproduced [6,10,11], the known transition strengths and the large α-decay width of the ground state are strongly underestimated [6,8,11,12]. The latter have been amended by strongly mixing shell-model and α-cluster configurations [13]. By including α clustering in the structure of the low-lying yrast states of ^{212}Po the known $B(E2)$ transition strengths have also been fairly well reproduced [14,15]. This led to the deduction that these states of ^{212}Po contain a large amount of α-cluster components [14–17].

In a recent study on ^{212}Po, Astier *et al.* [18] have observed several states at excitation energies above 1.7 MeV with non-natural parity which decay by enhanced $E1$ transitions. These transitions have been interpreted as fingerprints for the presence of large α-cluster components in the wave functions of these states. Concerning the low-lying yrast states, it was noted that the energies of the $2_1^+ - 4_1^+ - 6_1^+ - 8_1^+$ sequence can be considered as neutron-dominated two-particle excitations of the $(\pi h_{9/2})^2$ and the $(\nu g_{9/2})^2$ configurations in a similar fashion to the situation in ^{136}Te [19,20]. However, both the observed α-branching ratios [18] and the fact that the shell-model calculations underestimate the experimental

$B(E2)$ values for the decays of the 6_1^+ and the 8_1^+ states [6,8,11,12], have been interpreted as an indication for the presence of α-cluster components [18]. The findings in Ref. [18] have been advanced to a more refined theoretical description in the framework of a combined shell+α-cluster model [21]. In Ref. [21] all known properties of the yrast states of ^{212}Po were well reproduced and predictions for the $B(E2)$ values for the decays of 2_1^+ and the 4_1^+ states were made (cf. Table VI in Ref. [21]). We want to emphasize that the conclusions concerning the ability of shell models to describe the properties of the excited yrast states of ^{212}Po and the necessity to include α-cluster components in the structure of these states are solely based on the observed α-branching ratios [18] and the experimental $B(E2)$ values for the decays of the 6_1^+ and the 8_1^+ states. On the other hand, in a very recent study of ^{212}Po, it was shown that a phenomenological single-j shell model accounts very well for the properties of low-lying states, including also the off-yrast 2^+ isovector state [22]. At the same time, the α-branching ratios for the 4_1^+ and the 2_1^+ states are suppressed with respect to those for the 8_1^+ and the 6_1^+ states by factors of 6 and 100, respectively [18]. All of these properties raise the question whether α-cluster components are present in the structure of the 2_1^+ and the 4_1^+ states of ^{212}Po and whether shell models can describe consistently the electromagnetic properties of the $2_1^+ - 4_1^+ - 6_1^+ - 8_1^+$ sequence. To address these questions experimental information on the absolute $B(E2)$ strengths for the $2_1^+ \rightarrow 0_1^+$ and the $4_1^+ \rightarrow 2_1^+$ transitions is needed. This has motivated us to perform an experiment especially designed to measure the lifetime of the 2_1^+ state of ^{212}Po.

II. EXPERIMENTAL SETUP

The experiment was performed at the FN Tandem facility at the University of Cologne, Germany. The lifetime of the 2_1^+ state of ^{212}Po was measured by utilizing the RDDS method [23,24]. The excited states of ^{212}Po were populated using the α-transfer reaction ^{208}Pb(^{12}C,^{8}Be)^{212}Po. The target consisted of a 0.6-mg/cm^2 thin layer of Pb (enriched up to 99.14% with the isotope ^{208}Pb) evaporated on a 2-mg/cm^2 thick Au backing foil and was placed with the Au facing the beam. The beam energy of 64 MeV was chosen in such a way that the energy at which the reaction takes place after the Au backing to be about ∼62 MeV. The reaction was induced in the reaction chamber of the Cologne coincidence plunger device [25]. The stopper was a self-supporting 2-mg/cm^2 thick Au foil. Data were taken at six plunger distances: 25 μm, 35 μm, 43 μm, 55 μm, 70 μm, and 100 μm.

For detecting the light reaction fragments six solar cells (10 mm × 10 mm) were used. The array of solar cells was mounted in the plunger chamber at backward angles with respect to the beam axis, covering an angular range between 116.8° and 167.2°. The solar cells were placed at a distance of about 15 mm between their centers and the target. The γ rays from the decay of the excited states of ^{212}Po were registered by 11 HPGe detectors mounted outside the plunger chamber in two rings at a distance of, on average, 12 cm from the target. Five detectors were positioned at backward angles (142° with respect to the beam axis) and the other six detectors were placed at forward angles (45° with respect to the beam axis). Data were taken in coincidence mode of at least one solar cell and one HPGe detector (particle-γ) or when at least two HPGe detectors (γ-γ) were in coincidence.

III. DATA ANALYSIS AND RESULTS

The particle-γ coincidence data were sorted in 12 matrices depending on the positions of the HPGe detectors and the plunger distances. A projection of the particle-γ matrix obtained with γ-ray detection at 142° at plunger distance of 43 μm is shown in Fig. 1(a) as an example. The γ rays in coincidence with the group of particles indicated as "^{212}Po & ^{200}Tl" in Fig. 1(a) are shown in Fig. 1(b). This spectrum is dominated by transitions from excited states of ^{200}Tl which

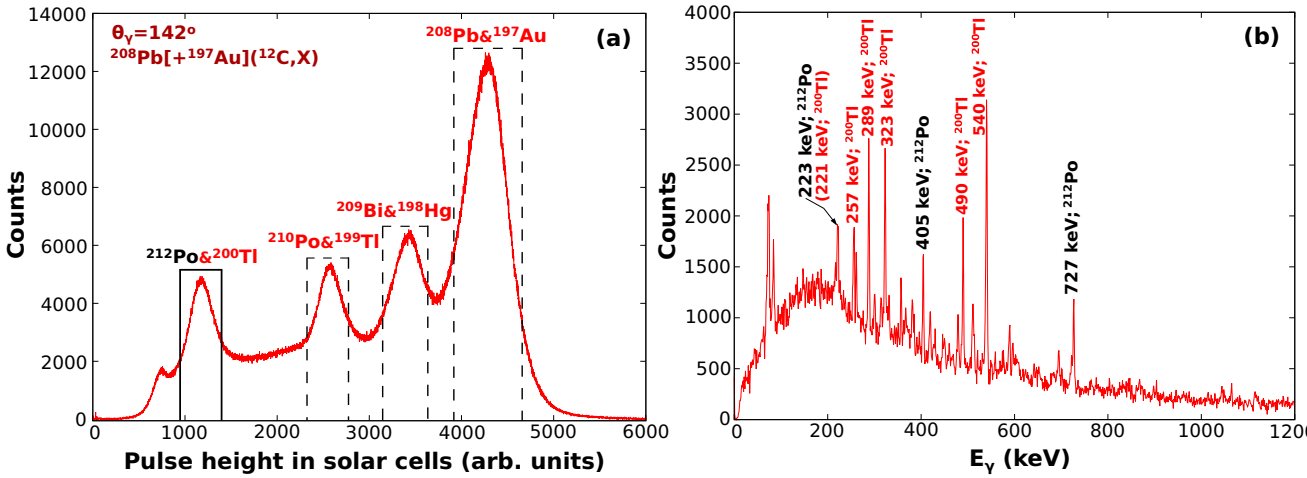

FIG. 1. (a) The projection of the particle-γ matrix obtained at plunger distance ($D = 43$ μm) by coincident detection of charged particles in the solar-cell array and a γ ray at a polar angle $\Theta_\gamma = 142°$. The marked ranges represent parts of the particle spectrum found to be in coincidence with the γ rays from the indicated nuclei. (b) The γ-ray spectrum in coincidence with the group of particles indicated as "^{212}Po and ^{200}Tl" in (a).

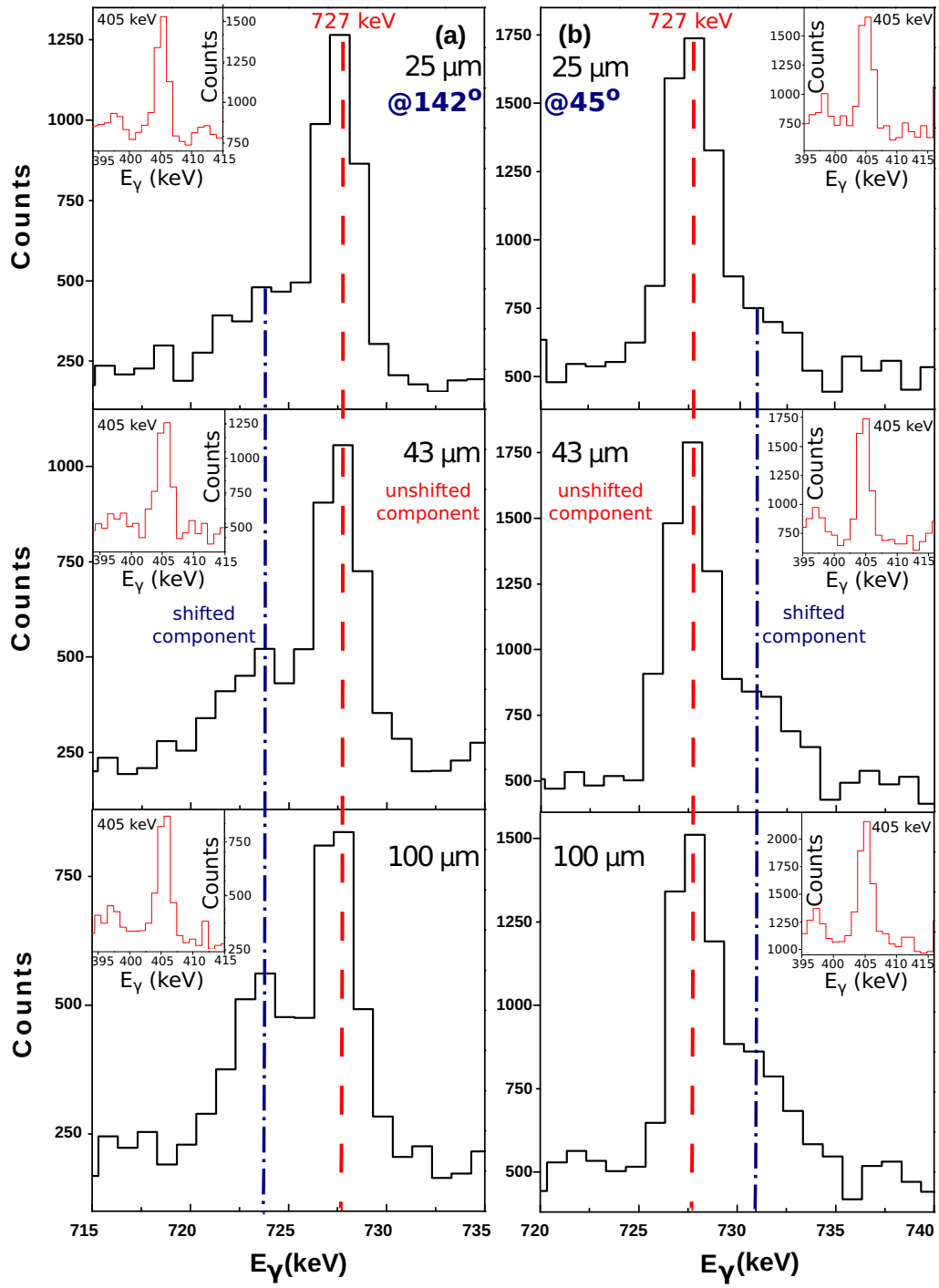

FIG. 2. Unshifted and shifted components of the 727-keV ($2_1^+ \rightarrow 0_1^+$) transition observed at backward angles (a) and at forward angles (b) for three different target-to-stopper distances: 25 μm, 43 μm, 100 μm. The dot-dashed lines (blue) represent the positions of the Doppler-shifted peak; the dashed lines (red) represent the unshifted peak positions. At the upper corners are shown the peaks of the 405-keV ($4_1^+ \rightarrow 2_1^+$) transition at the same detector angle and distance as those for the $2_1^+ \rightarrow 0_1^+$ transition.

is produced by the ^{197}Au(^{12}C,$2\alpha n$) transfer reaction in the backing or in the stopper. However, the 727-, 405-, and 223-keV lines which are the γ-ray transitions depopulating the first three yrast states of ^{212}Po [6,18,22] are also clearly visible. Moreover, it is also visible from Fig. 2 that the 727-keV transition between the 2_1^+ state of ^{212}Po and its ground state, has a well-pronounced shifted component which evolves as a function of plunger distance.

The evolution of the intensities of the shifted ($I_\gamma^{\rm sh}$) and the unshifted ($I_\gamma^{\rm un}$) components of the 727-keV line with respect to the change of the plunger distances is sensitive to the lifetime of the 2_1^+ state of ^{212}Po. The RDDS data for this transition

was analyzed by utilizing the differential decay curve method (DDCM) [26,27]. The standard application of DDCM requires the $I_\gamma^{\rm sh}$ and $I_\gamma^{\rm un}$ components (for each distance) to be measured from spectra in coincidence with Doppler-shifted components of transitions that feed directly the excited state of interest. Then the lifetime τ_i of the level of interest for the ith target-to-stopper distance depends on $I_{\rm sh}$ and $I_{\rm un}$ in the simple way [26,27]:

$$\tau_i(x) = \frac{I_{\rm un}(x)}{\langle v\rangle \frac{d}{dx} I_{\rm sh}(x)}, \qquad (1)$$

as here the derivative of the Doppler shifted intensities as a function of the target-to-stopper distance, $\frac{d}{dx} I_{\rm sh}$, is determined by a piecewise polynomial fit to the measured intensities $I_{\rm sh}$. For the present experiment this would require analyzing particle-γ-γ data which is not possible at the acquired level of statistics. However, the particular feeding pattern of the 2_1^+ state of ^{212}Po in the used transfer reaction allows this problem to be circumvented as described below.

Figure 2 shows particle-gated γ-ray spectra of the $2_1^+ \rightarrow 0_1^+$ transition observed at backward (a) and forward (b) angles at three different distances. The spectra are normalized with respect to the total number of counts in the particle gate [cf. Fig. 1(a)] and, as a result, the total number of counts in the 727-keV transition (the sum of the shifted and the unshifted components) remains constant for all distances. At the same time, the increase of the intensity of the shifted component $I_\gamma^{\rm sh}$ with increasing target-to-stopper distance is also apparent. However, the presented particle-gated spectra are, in fact, γ-ray singles spectra. Such spectra, in principal, only contain information for the so-called effective lifetime of the 2_1^+ state of ^{212}Po which aggregates the mean lifetime of the 2_1^+ state and the partial lifetimes of all states decaying to it. Therefore, the intensities of the $I_{\rm sh}$ and $I_{\rm un}$ components of the 727-keV transition derived from the spectra in Fig. 2 have to be corrected for the effects of the transitions feeding the 2_1^+ state. Because of the reaction mechanism it is justified to consider that slow feeding contributions to the effective lifetimes of excited states of ^{212}Po can originate only from discrete decays of higher-lying states, as suggested in Ref. [18]. The partial level scheme representing the known transitions directly populating the 2_1^+ state of ^{212}Po [6,18,22] is shown in Fig. 3. Amongst them only the 405-keV $4_1^+ \rightarrow 2_1^+$ transition can clearly be observed and its intensity can unambiguously be determined in our data [cf. Fig. 1(b)]. The reason for this is that the particle gated spectra in Fig. 1 is dominated by γ rays from ^{200}Tl produced by a transfer reaction in the backing of the plunger target. To estimate the relative contributions of the feeding transitions (cf. Fig. 3) to the intensity of the 727-keV ($2_1^+ \rightarrow 0_1^+$) transition we have used data from our previous study of ^{212}Po [22]. In Ref. [22] the same transfer reaction was utilized and as a result the same relative population of excited states of ^{212}Po can be expected. Indeed, the data from Ref. [22] show that the intensity ratio $I_\gamma(405\ {\rm keV}; 4_1^+ \rightarrow 2_1^+)/I_\gamma(727\ {\rm keV}; 2_1^+ \rightarrow 0_1^+)$ is 55.0(8)/100.0(5) while 54(9)/100(4) is measured in the present experiment. Using data from Ref. [22] we have estimated that 75% of the feeding of the 2_1^+ state comes from the states depicted in Fig. 3 as follows: 55% from the decay

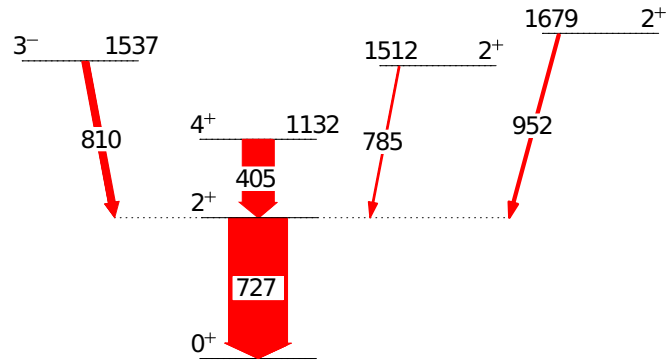

FIG. 3. Partial level scheme of ^{212}Po showing the excited states which feed the first excited 2^+ state directly. The thicknesses of the arrows are proportional to the observed γ -ray intensities.

of the 4_1^+ state at 1132-keV excitation energy, 4% from the decay of the 2_2^+ state at 1512 keV, 6% from the decay of the 2_3^+ state at 1679 keV, and 10% from the decay of the 3_1^- state at 1537 keV. Because no other γ rays feeding the 2_1^+ state are observed up to date, the remaining 25% of the intensity of the 727-keV transition is considered to originate from a direct population of the 2_1^+ state.

The lifetimes of the $2_{2,3}^+$ states of ^{212}Po were measured in our previous study [22] to be below 1 ps which means that they contribute only to the fast feeding of the 2_1^+ state. The lifetime of the 3^- state at 1537 keV is not known and cannot be determined from any of the available data sets. However, an $E1$ strength of about 1 mW.u. for the 810-keV transition (cf. Fig. 3) leads to a $\tau(3_1^-) \approx 0.5$ ps. Therefore, to simplify the discussion at this moment we assume that its lifetime is sufficiently short so that it decays only in flight. Nevertheless, the influence of the feeding from the 3^- state on the $\tau(2_1^+)$ will be discussed later. Under the above assumption the only essential feeder to the 2_1^+ state remains the 405-keV transition which depopulates the 4_1^+ state of ^{212}Po (cf. Fig. 3). It is expected that the 4_1^+ state has a long lifetime of about 140 ps, or longer [22]. This expectation is in agreement with the seniority-scheme behavior which further shows up in the very long lifetimes measured for the 6_1^+ [$\tau = 1.1(3)$ ns] [6] and the 8_1^+ [$\tau = 24.6(3)$ ns] [6] states of ^{212}Po. Indeed, as can be seen from the insets in Fig. 2 the 405-keV transition has only a stopped component for all plunger distances, i.e., the decay of the 4_1^+ state contributes only to the stopped component of the 727-keV transition. Hence, that extra contribution to the stopped component of the 727-keV transition has to be eliminated. In our analysis this was achieved by subtracting the efficiency-corrected number of counts in the 405-keV line out of the efficiency-corrected number of counts in the stopped component of the 727-keV transition (cf. Fig. 2). Under the considerations above, all other transitions feeding the 2_1^+ state (cf. Fig. 3) decay short-lived states ($\tau < 0.5$ ps). Hence, the intensities of the shifted components of the 727-keV transition being directly determined from the particle-gated spectra are not affected by the feeding transitions and consequently they are also related only to the lifetime of the 2_1^+ state of ^{212}Po.

It needs to be stressed that both $I_\gamma^{\rm un}$ and $I_\gamma^{\rm sh}$ being extracted with the procedure described above are natively bound to the

fast feedings of the 2_1^+ state, including one directly from the reaction. In this respect, they can be considered as effectively derived from γ-ray spectra in coincidence with the shifted components of all transitions directly feeding the state of interest. Therefore, they can be used to determine the lifetime of the 2_1^+ state with the DDCM, i.e., they can be used directly in Eq. (1).

To proceed with the DDCM analysis the mean velocity of the recoiling nuclei $\langle v \rangle$ has to be known. To make a realistic estimate of the mean velocity of the recoiling nuclei we have calculated the average drifting time of the recoiling nuclei in vacuum. The calculations are based on Monte Carlo simulations which account for all relevant stopping and straggling processes of the beam and the recoiling nuclei in the target, the experimental geometry, and the restrictions on the reaction kinematics imposed by the solar cell array. The simulations were carried out with the program APCAD (Analysis Programm for Continuous-Angle DSAM) [28]. In APCAD, the slowing down process is simulated by GEANT4 [29]. The electronic stopping powers were taken from the Northcliffe and Schilling tables [30] with corrections for the atomic structure of the medium, as discussed in Ref. [31]. The angular straggling from nuclear collisions is modeled discretely by means of Monte Carlo simulation while the corresponding energy loss is considered to emerge from a continuous process as the nuclear stopping powers were taken from SRIM2013 [32] and reduced by 30% [33]. Taking into account the reaction conditions as beam energy, backing and target thickness, and restrictions on the reaction kinematics imposed by the solar cells array, the ion drift times for all target-to-stopper distances were calculated from the simulated distributions and averaged over the distances. The average drifting time results in a mean velocity of the recoiling nuclei of $\langle v \rangle$ =0.75(10)%c. This value is in agreement with $\langle v \rangle$ =0.72(5)%c which was experimentally determined from the centroids of the shifted and the unshifted components of the 727-keV transition. Because the latter value is more precise, it was adopted and used in the DDCM analysis. The DDCM analysis for the lifetime of the 2_1^+ state of ^{212}Po with $\langle v \rangle$ =0.72(5)%c and intensities ($I_\gamma^{\rm un}$ and $I_\gamma^{\rm sh}$) extracted with the procedure described above is presented in Fig. 4 for forward and backward angles. The analysis results in a weighted mean value for the lifetime of the 2_1^+ state of 21.8(19) ps.

It has to be noted that the only assumption in the derivation of the above result which is not directly supported by experimental observations, is that the feeding from the 3_1^- state is fast (cf. Fig. 3). To investigate the influence of this feeding to the lifetime of the 2_1^+ state further, we have also

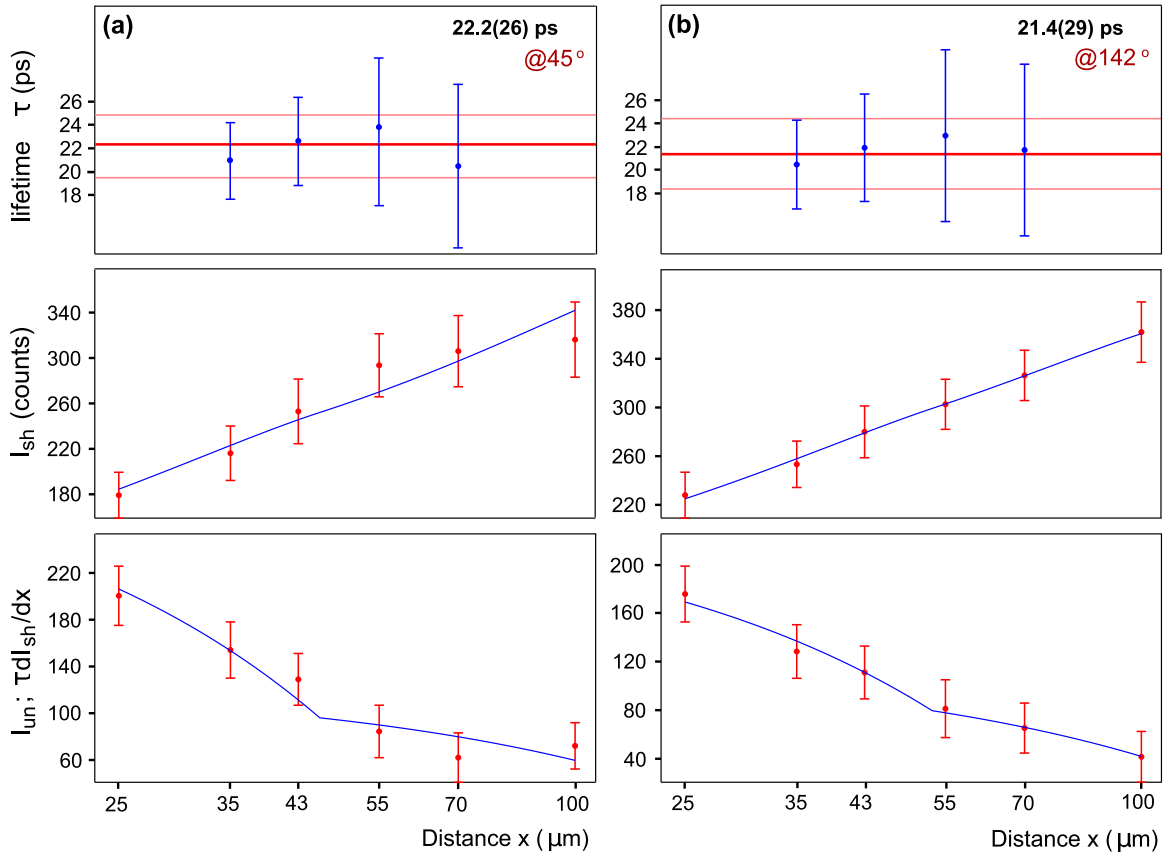

FIG. 4. The lifetime of the first excited 2^+ state of ^{212}Po determined at forward (a) and backward angles (b). The middle panels show the shifted intensities at different distances. Continuous curves are fitted through the points to calculate the derivative. In the bottom panels, curves that represent the product between the time derivatives of the shifted intensities and the lifetime of the level are compared with the experimental unshifted intensities. Out of this comparison, the lifetimes corresponding to each distance in the region of sensitivity are extracted, as seen in the upper panel. The horizontal lines represent the weighted mean values.

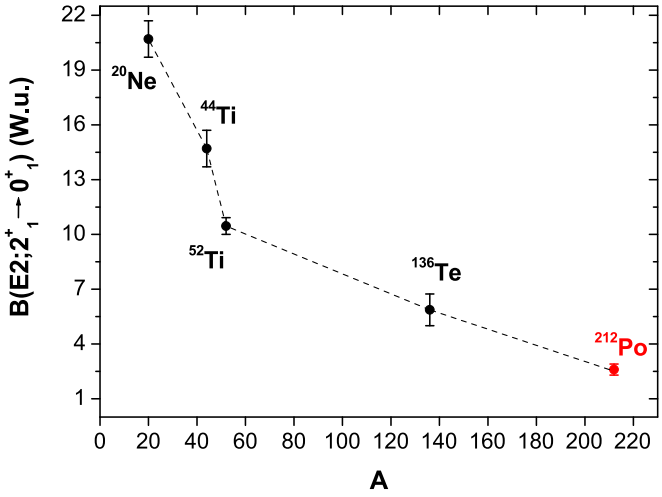

FIG. 5. The $B(E2;2_1^+ \rightarrow 0_1^+)$ values in Weisskopf units in nuclei having two valence protons and two valence neutrons. The data for ^{212}Po is from the present work. The other data is taken from [34]. The dashed line is drawn to guide the eye.

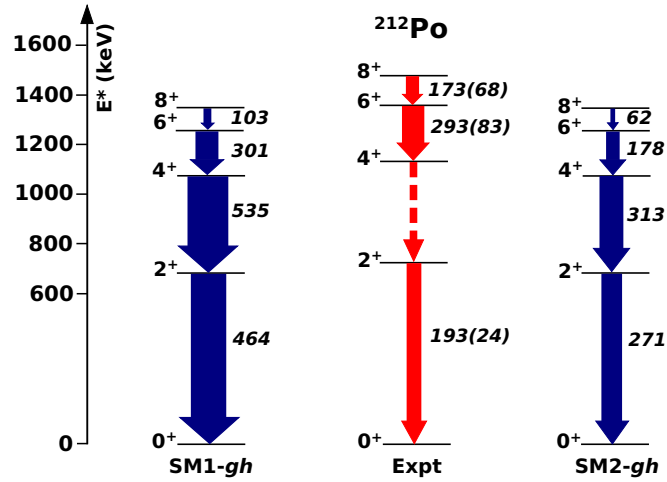

FIG. 6. A graphical representation of the results from Table I for the single-j shell-model calculations (SM1-gh and SM2-gh) for the low-lying states in ^{212}Po in comparison with experimental data (Expt). The thickness of the arrows is proportional to the $B(E2;2_1^+ \rightarrow 0_1^+)$ values in e^2fm^4. The latter are also presented by the numbers next to the arrows.

considered the alternative limit, i.e., we have assumed that the feeding from the 3_1^- state is very slow and contributes only to the unshifted component of the 727-keV transition. In this case, in addition to the intensity of the 405-keV transition, the intensity of the unshifted component of the 727-keV transition has to be reduced by an additional 10% which accounts for the intensity of the 810-keV transition ($3_1^- \rightarrow 2_1^+$; cf. Fig. 3). This alternative approach reduces the deduced lifetime of the 2_1^+ to 19.2(18) ps. For the final value for the lifetime of the 2_1^+ state we conservatively adopt the average value between the two limits which is

$$\tau(2_1^+, E_x = 727 \text{ keV}) = 20.5(26) \text{ ps}. \quad (2)$$

Taking into account the known electron conversion coefficient for the $2_1^+ \rightarrow 0_1^+$ transition of ^{212}Po [6] and the α-branching ratio of 0.033 [18], the newly derived lifetime of the 2_1^+ state translates to absolute transition strength $B(E2;2_1^+ \rightarrow 0_1^+) = 193(24)\ e^2fm^4 = 2.6(3)$ Wu.

IV. DISCUSSION

The measured size of the $B(E2;2_1^+ \rightarrow 0_1^+)$ value of 2.6(3) W.u. indicates a low collectivity in the structure of the 2_1^+ state of ^{212}Po. The value is about 2 times lower than the one measured in ^{136}Te [20] and, in fact, it is the lowest one ever measured in single-particle units in a nucleus having two valence protons and two valence neutrons as can be seen in Fig. 5.

The $B(E2;2_1^+ \rightarrow 0_1^+)$ value in ^{212}Po is a factor of about 2–3 times smaller than the available predictions of the α-clustering models [14,15,21] which may indicate absence of α-cluster components in the structure of the 2_1^+ state of ^{212}Po. However, the obtained experimental value is also more than a factor 2 times smaller than the calculated one in the framework of a single-j shell model [22]. Qualitatively, a comparatively low absolute transition strength from the 2_1^+ state of ^{212}Po can be expected in the framework of a single-j shell model because the wave function of the 2_1^+ state is expected to be neutron dominated, as shown in Ref. [22]. Then a plausible explanation for the discrepancy between the predicted and the measured $B(E2;2_1^+ \rightarrow 0_1^+)$ values (cf. Table I and SM1-gh in Fig. 6) could be sought in the choice of effective charges. The details about the single-j shell-model calculations are presented in Ref. [22]. There, the effective proton and neutron charges in the $E2$ transition operator were determined from the measured $B(E2;8_1^+ \rightarrow 6_1^+)$ values for ^{210}Pb and ^{210}Po [35,36] assuming the 6_1^+ and the 8_1^+ states of these nuclei have pure two-nucleon configurations. This approach yields effective charges of $e_\nu = 1.04e$ and $e_\pi = 1.52e$. For completeness, the resulting $B(E2)$ values for the lowest yrast states and the first isovector state (the 2_2^+ state) are presented in Ref. [22], in Table I, and in Fig. 6, labeled as SM1-gh. As it can be seen, the $B(E2)$ values for the decays of the 8_1^+ and the 6_1^+ states are reasonably well reproduced by the model approach SM1-gh while the experimental $B(E2;2_1^+ \rightarrow 0_1^+)$ value is significantly overestimated (cf. Fig. 6). Another approach is to determine the effective charges from the measured $B(E2;2_1^+ \rightarrow 0_1^+)$ values for ^{210}Pb and ^{210}Po [35,36] which leads to effective charges of $e_\nu = 0.83e$ and $e_\pi = 1.09e$. The results from these calculations are presented in Table I and in Fig. 6, labeled as SM2-gh. Not surprisingly, the calculated $B(E2;2_1^+ \rightarrow 0_1^+)$ value for ^{212}Po is closer to our experimental one. It is also worth noting that such an improvement in the description of the $B(E2;2_1^+ \rightarrow 0_1^+)$ value leads to a perfect agreement between the experimental and the calculated $B(E2;2_2^+ \rightarrow 0_1^+)$ values (cf. Table I). This, however, can be expected because the 2_2^+ state is the isovector partner of the 2_1^+ state, i.e., these two states of ^{212}Po have almost identical wave functions as the main difference between them is a phase factor [22]. On the other hand, the results for the transition strengths for the 8_1^+ and the 6_1^+ (cf. SM2-gh in Fig. 6) states are about a factor of

TABLE I. Comparison between the experimental and calculated (see text for details) properties of the low-lying states in ^{212}Po. The experimental $B(E2)$ values are from Refs. [7,18], unless otherwise specified.

J_i^π	E_x (MeV)		J_f^π	$B(E2; J_i \to J_f)$(e^2 fm^4)		
	Expt	SM-gh		Expt	SM1-gh[a]	SM2-gh[b]
2_1^+	0.727	0.690	0_1^+	193(24)[c]	464	271
4_1^+	1.132	1.081	2_1^+	—	535	313
6_1^+	1.355	1.261	4_1^+	293(83)	301	178
8_1^+	1.475	1.350	6_1^+	173(68)	103	62
2_2^+	1.512	1.363	0_1^+	29(4)[d]	59	27
			2_1^+	24(16)[d]	17	8

[a]With $e_\pi = 1.52e$ and $e_\nu = 1.04e$.
[b]With $e_\pi = 1.09e$ and $e_\nu = 0.83e$.
[c]From the present work.
[d]From Ref. [22].

two lower than the experimental ones. This analysis suggests that agreement between experimental and simple single-j shell model cannot be achieved for the $B(E2)$ rates by adjusting the effective charges.

Because the single-j shell-model calculations use an empirical effective interaction derived from the spectra of ^{210}Pb, ^{210}Bi, and ^{210}Po, it is interesting to check whether the problem in the description of the $E2$ transition strengths between the yrast states of ^{212}Po is also present in ^{210}Pb and ^{210}Po. Results from the single-j shell-model calculations for these $B(E2)$ values in ^{210}Pb and ^{210}Po are presented in Tables II and III under the columns labeled SM1-gh and SM2-gh. The labeling of the columns reflects the approach in choosing the effective charges in the same way as in Table I. The problem is clearly present for both nuclei—if the effective charges are fixed to the $B(E2; 8_1^+ \to 6_1^+)$ values (SM1-gh), the $B(E2; 2_1^+ \to 0_1^+)$ values are overestimated, otherwise, if the effective charges are fixed to the $B(E2; 2_1^+ \to 0_1^+)$ values (SM2-gh), the $B(E2; 8_1^+ \to 6_1^+)$ and the $B(E2; 6_1^+ \to 4_1^+)$ values are underestimated. The situation looks slightly better in ^{210}Po where the $B(E2; 4_1^+ \to 2_1^+)$ value is reproduced in SM1-gh calculations (see Table III) while for ^{210}Pb this value

TABLE II. Comparison between the experimental and calculated (see text for details) properties of the yrast states in ^{210}Pb. The experimental excitation energies and $B(E2)$ values are from Ref. [35].

J_i^π	E_x (MeV)		$B(E2; J_i \to J_f)$(e^2 fm^4)				
	Expt	SM	J_f^π	Expt	SM1-gh[a]	SM2-gh[b]	SM[b]
2_1^+	0.800	0.837	0_1^+	105(30)	166	106	109
4_1^+	1.098	1.099	2_1^+	360(68)	191	121	144
6_1^+	1.195	1.191	4_1^+	158(60)	132	84	101
8_1^+	1.278	1.234	6_1^+	53(23)	53	34	43

[a]With $e_\nu = 1.04e$.
[b]With $e_\nu = 0.83e$.

TABLE III. Comparison between the experimental and calculated (see text for details) properties of the yrast states in ^{210}Po. The experimental excitation energies and $B(E2)$ values are from Ref. [35], unless otherwise specified.

J_i^π	E_x (MeV)		$B(E2; J_i \to J_f)$(e^2 fm^4)				
	Expt	SM	J_f^π	Expt	SM1-gh[a]	SM2-gh[b]	SM[b]
2_1^+	1.181	1.200	0_1^+	136(21)[c]	263	137	133
4_1^+	1.427	1.466	2_1^+	335(14)	302	157	169
6_1^+	1.473	1.482	4_1^+	229(7)	209	109	116
8_1^+	1.557	1.533	6_1^+	84(3)	84	44	46

[a]With $e_\pi = 1.52e$.
[b]With $e_\pi = 1.09e$.
[c]From Ref. [36].

is underestimated by a factor of 2 or more in both calculations (see Table II). However, the results from the SM1-gh and SM2-gh clearly demonstrate that whatever the procedure for choosing the effective charges, the single-j shell model cannot provide a consistent description of the $B(E2)$ values for the yrast states of ^{210}Pb and ^{210}Po and, consequently, it cannot be expected that the same model will perform better at describing the $B(E2)$ values in ^{212}Po (cf. Table I and Fig. 6).

At this point, it can be speculated that the failure of the single-j shell model in the cases of ^{210}Po and ^{210}Pb originates from the extremely limited model space. To check this hypothesis we have performed realistic shell-model calculations. The valence space consists of all neutron orbitals in the 126-184 shell ($3s_{1/2}$, $2d_{3/2}$, $2d_{5/2}$, $1g_{7/2}$, $1g_{9/2}$, $0h_{11/2}$, and $0j_{15/2}$) and all proton orbitals in the 82-126 shell ($2p_{1/2}$, $2p_{3/2}$, $1f_{5/2}$, $1f_{7/2}$, $0h_{9/2}$, and $0i_{13/2}$). The Kuo-Herling interaction [37], which is an effective interaction tailored for this model space, is used to calculate properties of nuclei with two valence nucleons beyond ^{208}Pb. The single-particle energies are those given by Warburton and Brown [38]. The effective proton and neutron charges are the same as in the SM2-gh calculations. The results for both ^{210}Pb and ^{210}Po are presented in Tables II and III, respectively, as well as in Fig. 7, labeled as SM.

The realistic shell model (SM) reproduces almost perfectly the energies of the yrast states in ^{210}Pb and ^{210}Po (cf. Fig. 7). However, in both cases the description of the $B(E2)$ values is only marginally improved with respect to the ones obtained in the single-j shell-model calculation SM2-gh (cf. Tables II and III). In this respect, it cannot be expected that realistic shell-model calculations will improve the description of the low-lying yrast states of ^{212}Po. The problem with the inconsistency in the description of the $B(E2)$ values between the yrast states of ^{210}Po [39] also exists in ^{210}Pb and it is not specific for shell models only [36]. A reason for this inconsistency might be a softness of the ^{208}Pb core which facilitates the 1-ph excitations which are not fully accounted in these shell-model spaces as suggested in Ref. [39]. Apparently, the key for understanding the structure of the low-lying yrast states of ^{212}Po which show unexpectedly low collectivity, lies in the understanding of the behavior of the seniority-2 configurations in ^{210}Pb and ^{210}Po.

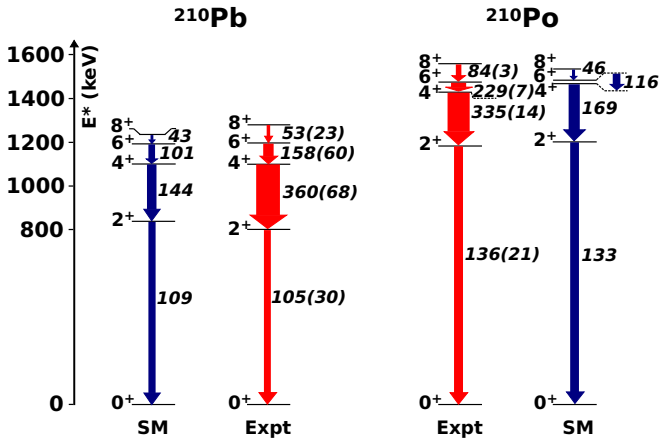

FIG. 7. A graphical representation of the results from Tables II and III for realistic shell-model calculations (SM) for the low-lying states in ^{210}Pb and ^{210}Po in comparison with experimental data (Expt). The thickness of the arrows is proportional to the $B(E2; 2_1^+ \rightarrow 0_1^+)$ values in e^2fm^4. The latter are also presented by the numbers next to the arrows.

V. SUMMARY

We have measured the lifetime of the 2_1^+ state of ^{212}Po by utilizing the RDDS method in an α-transfer reaction experiment. The extracted low $B(E2)$ value shows low collectivity and does not support the suggestion for presence substantial α-cluster components in the structure of the state. The low collectivity implies that appropriate theoretical understanding of the structure of the low-lying yrast states of ^{212}Po could be achievable within the framework of nuclear shell models. However, the performed shell-model calculations have shown that, while the energies of the states can be reproduced very well, no consistent description of the known $B(E2)$ values could be obtained. This problem appears to originate from the properties of the seniority-2 configurations in ^{210}Pb and ^{210}Po. More thorough theoretical investigations of the low-energy structures of $A = 210$ isobars are needed.

ACKNOWLEDGMENTS

D.K. acknowledges the support from Deutscher Akademischer Austauschdienst. G.R. acknowledges the support from the Alexander von Humboldt foundation. This work was supported by the partnership agreement between the University of Cologne and University of Sofia, by the Bulgarian National Science Fund under Grant No. DN08/23/2016, by the Science and Technology Facilities Council, and by the Bundesministerium für Bildung und Forschung under Grants No. 05P12RDCIB, No. 05P15RDFN1/9, and No. 05P15RDCIA.

[1] M. G. Mayer, Phys. Rev. **78**, 16 (1950).
[2] R. F. Casten, Phys. Lett. B **152**, 145 (1985).
[3] I. Perlman, F. Asaro, A. Giorso, A. Larsh, and R. Latimer, Phys. Rev. **127**, 917 (1962).
[4] N. Auerbach and I. Talmi, Phys. Lett. **10**, 297 (1964).
[5] R. M. Lieder, J. P. Didelez, H. Beuscher, D. R. Haenni, M. Müller-Veggian, A. Neskakis, and C. Mayer-Böricke, Phys. Rev. Lett. **41**, 742 (1978); P. A. Baisden, R. E. Leber, M. Nurmia, J. M. Nitschke, M. Michel, and A. Ghiorso, *ibid.* **41**, 738 (1978); P. Lemmertz *et al.*, Z. Phys. A **298**, 311 (1980).
[6] A. R. Poletti *et al.*, Nucl. Phys. A **473**, 595 (1987).
[7] E. Browne, Nucl. Data Sheets **104**, 427 (2005) and the references therein.
[8] I. Tonozuka and A. Arima, Nucl. Phys. A **323**, 45 (1979).
[9] F. A. Janouch and R. J. Liotta, Phys. Rev. C **25**, 2123 (1982).
[10] D. Strottman, Phys. Rev. C **20**, 1150 (1979).
[11] E. K. Warburton, Phys. Rev. C **44**, 261 (1991).
[12] G. Dodig-Crnkovic, F. A. Janouch, and R. J. Liotta, Phys. Lett. B **139**, 143 (1984).
[13] K. Varga, R. G. Lovas, and R. J. Liotta, Phys. Rev. Lett. **69**, 37 (1992).
[14] F. Hoyler, P. Mohr, and G. Staudt, Phys. Rev. C **50**, 2631 (1994).
[15] B. Buck, J. C. Johnston, A. C. Merchant, and S. M. Perez, Phys. Rev. C **53**, 2841 (1996).
[16] B. Buck, A. C. Merchant, and S. M. Perez, Phys. Rev. Lett. **72**, 1326 (1994).
[17] S. Ohkubo, Phys. Rev. Lett. **74**, 2176 (1995).
[18] A. Astier, P. Petkov, M.-G. Porquet, D. S. Delion, and P. Schuck, Phys. Rev. Lett. **104**, 042701 (2010); Eur. Phys. J. A **46**, 165 (2010).
[19] D. C. Radford *et al.*, Phys. Rev. Lett. **88**, 222501 (2002).
[20] M. Danchev *et al.*, Phys. Rev. C **84**, 061306(R) (2011).
[21] D. S. Delion, R. J. Liotta, P. Schuck, A. Astier, and M.-G. Porquet, Phys. Rev. C **85**, 064306 (2012).
[22] D. Kocheva *et al.*, Phys. Rev. C **93**, 011303(R) (2016).
[23] T. K. Alexander and J. S. Forster, Adv. Nucl. Phys. **10**, 197 (1978).
[24] A. Z. Schwarzschild and E. K. Warburton, Annu. Rev. Nucl. Sci. **18**, 265 (1968).
[25] A. Dewald, O. Möller, and P. Petkov, Prog. Part. Nucl. Phys. **67**, 786 (2012).
[26] A. Dewald, S. Harissopulos and P. von Brentano, Z. Phys. A **334**, 163 (1989).
[27] G. Böhm, A. Dewald, P. Petkov and P. von Brentano, Nucl. Instrum. Methods A **329**, 248 (1993).
[28] C. Stahl, J. Leske, M. Lettmann, and N. Pietralla, Comput. Phys. Commun. **214**, 174 (2017).
[29] S. Agostinelli *et al.*, Nucl. Instrum. Methods Phys. Res., Sect. A **506**, 250 (2003).
[30] L. C. Northcliffe and R. F. Schilling, Nucl. Data Sect. **7**, 233 (1970).
[31] J. F. Ziegler and J. P. Biersack, in *Treatise on Heavy Ion Science*, edited by D. A. Bromley (Plenum Press, New York, 1985), Vol. 6, p. 95.
[32] J. F. Ziegler, M. D. Ziegler, and J. P. Biersack, Nucl. Instrum. Methods B **268**, 1818 (2010).
[33] J. Keinonen, AIP Conf. Proc. **125**, 557 (1985).
[34] S. Raman, C. W. Nestor, Jr., and P. Tikkanen, At. Data Nucl. Data Tables **78**, 1 (2001); [http://www.nndc.bnl.gov/ensdf/].

[35] M. Shamsuzzoha Basunia, Nucl. Data Sheets **121**, 561 (2014).
[36] D. Kocheva *et al.*, Eur. Phys. J. A **53**, 175 (2017).
[37] G. H. Herling and T. T. S. Kuo, Nucl. Phys. A **181**, 113 (1979).
[38] E. K. Warburton and B. A. Brown, Phys. Rev. C **43**, 602 (1991).
[39] E. Caurier, M. Rejmund, and H. Grawe, Phys. Rev. C **67**, 054310 (2003).